12

Dispersion of a Laser Pulse at Propagation Through an Image Acquisition System

Toadere Florin
INCDTIM Cluj Napoca
Romania

1. Introduction

The purpose of this chapter is to analyze different lenses and fibers, in order to find the best solution for the compensation of the laser pulse dispersion. We generate a laser pulse which is captured by an image acquisition system. The system consists of a laser, an optical fiber and a CMOS senor. In figure 1, we use a confocal resonator to generate the laser pulse; then the generated light is focused into an optical fiber using a lens; the light is propagated through the fiber and at the output of the fiber the light is projected on a CMOS sensor. For the same system, we propose three different combinations in which different lenses and fibers are used in order to compensate the dispersion of a laser pulse at propagation through the image acquisition system. Laser generates Hermite Gaussian modes. We use the fundamental mode which is the Gaussian pulse. This pulse spreads at propagation through the free space. In order to avoid the spreading, we focus the pulse into an optical fiber using different lenses. Also the lenses suffer of chromatic dispersion. In order to decrease the effect of the chromatic dispersion, we design and analyze the functionality of a singlet, an achromatic doublet and an apochromat. At the output of the lens the pulse is focalized into an optical fiber. We take in consideration the step index fiber, the graded index fiber and self phase modulation fiber. The step index fiber suffers of intermodal dispersion, an alternative solution is to use the grade index fiber and the best solution is provided by the self phase modulation fiber. Finally, at the output of the fiber the light spreads on the CMOS sensor. During the functionality of the senor it introduces different temporal and spatial noises which degrade the quality of the pulse. Consequently, we have to reconstruct the image of the pulse using the Laplace, the amplitude and the bilateral filters.

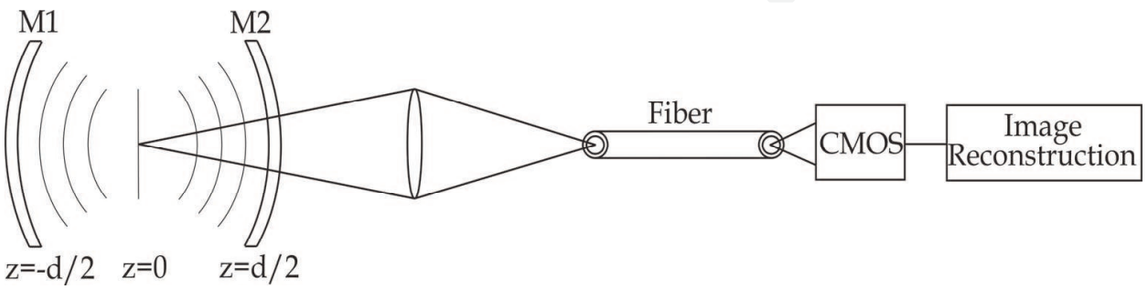

Fig. 1. A schematic of the image capture system

2. The laser modes

In order to find the laser modes we consider a confocal resonator system like that in figure 1. The optical axis is noted with *z*, and the light propagates from left to right in report with the optical axis. The resonator is made by two concave mirrors of equal radii of curvature $R = \frac{d}{2}$ separated by a distance *d*, and one mirror is a partially refractive mirror M_2. We consider the middle of the resonator in the point $z = -\frac{d}{2} + \frac{d}{2} = 0$. After certain calculus (Poon & Kim, 2006), the modes in the middle of the resonator can be express as:

$$\psi(x, y, z = 0) = E_0 \exp\left[-\frac{\left(x^2 + y^2\right)}{w_0^2} \right] \cdot H_m\left(\frac{\sqrt{2}x}{w_0} \right) H_n\left(\frac{\sqrt{2}y}{w_0} \right) \tag{1}$$

where:
w_0 is the waist of the beam,
H_m is the Hermite Gaussian polynomial,

$$H_m(x) = (-1)^m e^{x^2} \frac{d^m}{dx^m} e^{-x^2} \ . \tag{2}$$

We have the 2D solution represented in figure 2 (Toadere & Mastorakys 2009, 2010).

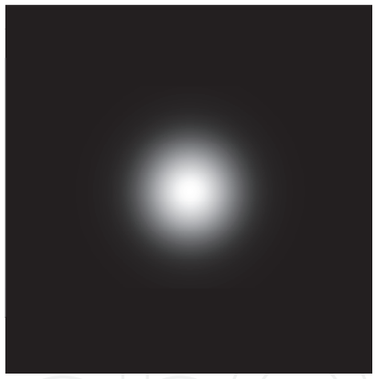

Fig. 2. The fundamental Hermite Gaussian mode TEM_{00}

Each set (*m*,*n*) corresponds to a particular transverse electromagnetic mode of the resonator. The electric (and magnetic) field of the electromagnetic wave is orthogonal in the middle of the resonator in point $z = 0$. The lowest-order Hermite polynomial H_0 is equal to unity; hence the mode corresponding to the set (0,0) is called the TEM_{00} mode and has a Gaussian radial profile. The laser output comprises a small fraction of the energy in the resonator that is coupled out through a partially refractive mirror. The width of the Gaussian beam monotonically increases in function of propagation on direction *z*, and reaches $\sqrt{2}$ times its original width at Rayleigh range. For a circular beam, this means that the mode area is doubled at this point (Poon & Banarje, 2001), (Poon & Kim, 2006).
In this paper we consider that the laser generates a pulse with a Gaussian radial profile (TEM_{00}). To avoid the spreading of the pulse, in the Rayleigh range at 20*mm*, we focus the

pulse in to a fiber using a lens. In order to attenuate the chromatic dispersion we use the singlet, the doublet, the apochromat, and the step fiber, the graded index fiber and the non linear index fiber.

3. The optical system analysis

When we work with optical components, the most important problem is that it is impossible to image a point object as a perfect point image. An optical system is made by a set of components (surfaces) through which the light passes. The optical sensor is analyzed in space by the point spread function (PSF) and in the spatial frequency by the modulation transfer function (MTF). These are the most important integrative criterions of imaging evaluation for the optical system. The PSF gives the 2D intensity distribution of the image of a point source. PSF gives the physically correct light distribution in the image plane including the effects of aberrations and diffraction. Errors are introduced by design (geometrical aberrations), optical and mechanical fabrication or alignment. MTF characterize the functionality of the optical system in spatial frequencies. Most optical systems are expected to perform a predetermined level of image integrity. A method to measure this quality level is the ability of the optical system to transfer various levels of details from the object to the image. This performance is measured in terms of contrast or modulation, and is related to the degradation of the image of a perfect source produced by a lens. MTF describe the image structure as a function of spatial frequency and is specified in lines per millimeter. It is obtained by Fourier transform of the image spatial distribution (Goodmann, 1996), (Yzuka, 2008).

When an optical system process an image using incoherent light, then the function which describe the intensity in the image plane produced by a point in the object plane is called the impulse response function:

$$g(x,y) = H\left[f(x,y) \right] \tag{3}$$

H is an operator representing a linear, position (or space) invariant system. The input object intensity pattern and the output image intensity pattern are related by a simple convolution equation:

$$g(x,y) = \int_{-\infty}^{+\infty}\int f(\alpha,\beta) H\left[\delta\left((x-\alpha, y-\beta) \right) \right] d\alpha d\beta \,,\; g(x,y) = \int_{-\infty}^{+\infty}\int f(\alpha,\beta) h(x-\alpha, y-\beta) d\alpha d\beta \,, \tag{4}$$

α and β are spatial frequencies (line/mm) which are defined as the rate of repetition of a particular pattern in unit distance.

$$h(x-\alpha, y-\beta) = H\left[\delta(x-\alpha, y-\beta) \right] \tag{5}$$

is the impulse response of H; in optics, it is called the point spread function (PSF). The net PSF of the optical part of the image acquisition system is a convolution between the individual responses of the optical components: the lens, the fiber and the optical part of the CMOS:

$$PSF = PSF_{lens} * PSF_{fiber} * PSF_{CMOS} \;. \tag{6}$$

We work with multiple convolutions, and we focus our attention on space analysis using the point spread function, which is specific to each component of the optical sensor. The optical fiber is analyzed from the spatial resolution point of view (Toadere & Mastorakis, 2009, 2010).
The PSF characterize the image analyses in space but also we can characterize the image in frequency using the optical transfer function (OTF) (Yzuka, 2008). The optical transfer function is the normalized autocorrelation of the transfer function and has the formula:

$$H(\alpha,\beta)=\frac{\iint P\left(x+\frac{\alpha}{2},y+\frac{\beta}{2},\right)P\left(x-\frac{\alpha}{2},y-\frac{\beta}{2},\right)}{\iint P(x,y)^2\,dxdy}. \tag{7}$$

The numerator represents the area of overlap of two pupil functions, one of which is displaced by $\frac{\alpha}{2},\frac{\beta}{2}$ and $-\frac{\alpha}{2},-\frac{\beta}{2}$ in directions x an y and the other in opposite directions $-x$ and $-y$. OTF is defined as the rapport between the area of the overlap of displace pupil function and complete area of the pupil function.
The changes in contrast that happens when an image passes trough an optical system is expected to have a lot to do with the optical transfer function (Goodmann, 1996) (Yzuka, 2008), (Toadere & Mastorakis, 2010). The definition of the modulation transfer function (MTF) is:

$$MTF=\frac{contrast\quad of\quad output\quad image}{contrast\quad of\quad input\quad image} \tag{8}$$

which represent the ratio of the contrast of the output image to that of the input image.
The relation between OTF and MTF is:

$$MTF=\left|OTF\right|. \tag{9}$$

The modulation transfer function is identical to the absolute value of the optical transfer function. The net sensor MTF is a multiplication between the transfer functions of the individual components:

$$MTF=MTF_{lens}\times MTF_{fiber}\times MTF_{CMOS}. \tag{10}$$

In general, the contrast of any image which has propagated through an image acquisition system is worse then the contrast of the original input image.

3.1 The PSF and MTF with aberrations

When we work with real optical systems, which have aberrations, the point spread function the optical transfer function and the modulation transfer function suffers modifications due to a phase distortion term $W(x,y)$ (Goodmann, 1996):

$$PSF=\frac{1}{\lambda^2 d^2 A_p}\left\|FT\left\{p(x,y)\cdot e^{-\frac{2x}{\lambda}W(x,y)}\right\}\right|_{f_x=\frac{x}{\lambda d},f_y=\frac{y}{\lambda d}}\Bigg\| \tag{11}$$

where:
λ is the wavelength,
FT is the Fourier transform,
d is the distance from the aperture to the image plane,
A_p is the area of the aperture,
$W(x,y)$ is the aberration of the pupil,
$p(x,y)$ is the pupil function,

$$P(x,y) = p(x,y) \cdot e^{-\frac{2x}{\lambda}W(x,y)} . \tag{12}$$

The optical transfer function is:

$$OTF(f_x, f_y) = \frac{FT(PSF)}{FT(PSF)\Big|_{f_x=0, f_y=0}} \tag{13}$$

and the modulation transfer function is:

$$MTF(f_x, f_y) = \left| OTF(f_x, f_y) \right| . \tag{14}$$

3.2 The monochromatic aberrations

Aberrations are the failure of light rays emerging from a point object to form a perfect point image after passing through an optical system. Aberrations lead to blurring of the image, which is produced by the image-forming optical system. The wave front emerging from a real lens is complex because has error in the design, fabrication and lens assembly. Nevertheless, well made and carefully assembled lenses can possess certain inherent aberrations. To describe the primary monochromatic aberrations, of rotationally symmetrical optical systems, we specify the shape of the wave front emerging from the exit pupil. For each object point, there will be a quasi-spherical wave front converging toward the paraxial image point (Goodmann, 1996), (Kidger, 2001).

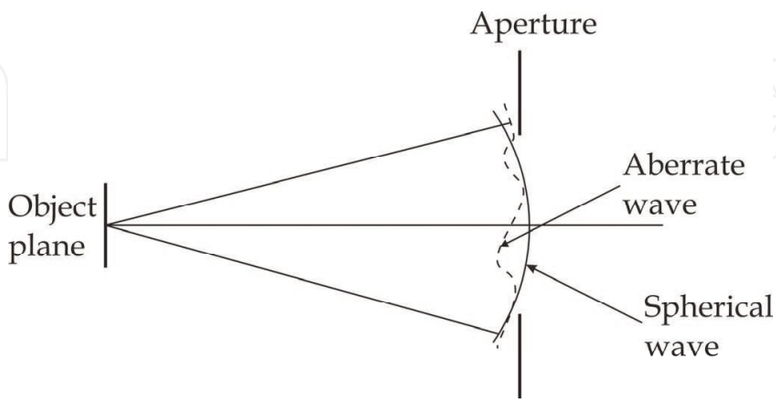

Fig. 3. The wavefront aberrations

In figure 3 the wave aberration function, W(x,y), is the distance, in optical path length, from the reference sphere to the wavefront in the exit pupil measured along the ray as a function

of the transverse coordinates (x,y) of the ray intersection with a reference sphere centered on the ideal image point.
To specify the aberrations we use the Siedel field aberration formula:

$$W(r,\theta) = W_{020}r^2 + W_{040}r^4 + W_{131}hr^3\cos(\theta) + \\ +W_{220}h^2r^2 + W_{311}h^3r\cos(\theta) + (higher \quad order \quad terms) \tag{15}$$

where:
W_{klm} are the wave aberration coefficients of the modes,
h is the height of the object,
r^2 is the defocus,
r^4 is the spherical aberration,
$hr^3\cos(\theta)$ is the coma,
$h^2r^2\cos^2(\theta)$ is the astigmatism,
h^2r^2 is the field curvature,
$h^3r\cos(\theta)$ is the distortion.

This Seidel aberration formula represents orthogonal polynomials which have the next properties: field aberrations describe the wavefront for a single object point as a function of pupil coordinates (*x,y*) and field height *h*. The aberrations are described functionally as a linear combination of polynomials. Point aberrations depend only on pupil coordinates and each polynomial term represents a single aberration. The aberration polynomial may be extended to higher order; these aberrations presented in equation (15) are up to fourth order. (Kidger 2001).
The Siedel aberrations for thin lenses can be express in function of bending and magnification (Geary, 2002), (Kidger, 2001). The bending can be express in function of the thin lens curvature:

$$B = \frac{c_1 + c_2}{c_1 - c_2}. \tag{16}$$

From the formula of the Lagrange invariant, the transverse magnification is given by:

$$m = \frac{y'}{y} = \frac{nu}{n'u'} \tag{17}$$

and the magnification is:

$$M = \frac{m+1}{m-1}. \tag{18}$$

Consequently, the Siedel aberrations are: W_{040} is the spherical aberration, W_{131} is the coma, W_{222} the astigmatism, W_{220} the field curvature, W_{311} is the distortion, W_{020} is the axial color and W_{111} is the lateral color:

$$W_{040} = \frac{1}{16}y_a^2\phi^3(a_1 + a_2(B - a_3M)^2 - a_4M^2), \tag{19}$$

$$W_{131} = \frac{1}{4\lambda} y_a^2 \phi^2 L(a_5 B - a_6 M), \tag{20}$$

$$W_{222} = \frac{1}{2\lambda} L^2 \phi, \tag{21}$$

$$W_{220} = \frac{1}{4\lambda} L^2 \phi \frac{n_g + 1}{n_g}, \tag{22}$$

$$W_{311} = 0, \tag{23}$$

$$W_{020} = \frac{1}{2\lambda} y_a^2 \frac{\phi}{\nu}, \tag{24}$$

$$W_{111} = 0 \tag{25}$$

where:

y_a is the aperture,

ϕ is the lens power,

ν is the Abbe number,

n_g are the glass refraction indices,

$L = -nu_a y_c$ is the Lagrange invariant,

$B = \frac{c_1 + c_2}{c_1 - c_2}$ is the bending, $M = \frac{1+m}{1-m}$ is the magnification,

$$a_1 = \left(\frac{n_g}{n_g - 1} \right)^2,\ a_2 = \frac{n_g + 2}{n_g (n_g - 1)^2},\ a_3 = \frac{2(n_g^2 - 1)}{n_g + 2},\ a_4 = \frac{n_g}{n_g + 2},\ a_5 = \frac{n_g + 1}{n_g (n_g - 1)},\ a_6 = \frac{2n_g + 1}{n_g}.$$

3.3 The correction of the aberrations

In the paragraph 3.2, we presented the mathematical relations that are used in the optical design which implies Seidel aberrations (Kidger, 2004), (Toadere & Mastorakis, 2010). In order to optimize the defects produced by the aberrations we use the defect vector f which is a set of m functions f_i that depend on a set on n variables. The function is of the type:

$$\sigma^2 = f^t \cdot f\ . \tag{26}$$

A is a $(n \times m)$ matrix of first derivatives:

$$A_{ij} = \frac{\partial f_i}{\partial x_j} \tag{27}$$

and f are changes in the variables from the current design. The gradient g is a $(n \times 1)$ vector given by:

$$g = \frac{1}{2}\nabla\sigma^2 \tag{28}$$

its components are:

$$g_i = \frac{\partial\sigma^2}{\partial x_i} = 2\left(f_1\frac{\partial f_1}{\partial x_i} + f_2\frac{\partial f_2}{\partial x_i} + \ldots f_m\frac{\partial f_m}{\partial x_i}\right), \tag{29}$$

$$g = A^t f.$$

Method of Least Squares:

$$g = A^t(f_0 + As),$$

$$g = g_0 + A^t As,$$

$$C = A^t A,$$

$$g_0 + Cs = 0.$$

is a set of simultaneous linear equations known as the normal equations of least-squares. Providing that the matrix C is not singular, these equations can always be solved, and the formal solution s may be written:

$$s = -C^{-1}g_0. \tag{30}$$

The basic idea of the damped least-squares is to start with the basic equation for the least squares condition. g_0 is the gradient at the starting point and augment the diagonal of the matrix C by the addition or factoring of a damping coefficient. Modifications of the form $c_{ii} + p$ for example, are called additive damping. In the case of additive damping, the equation for the damped least-squares solution reduces to:

$$g_0 + ps + Cs = 0. \tag{31}$$

As the damping factor p increases, the third term in the equation above becomes small and the solution vector becomes parallel to the gradient vector:

$$s = -\frac{1}{p}g_0 \tag{32}$$

3.4 The lens design

Lens design refers to the calculation of lens construction parameters that will meet a set of performance requirements and constraints. Construction parameters include surface profile types and the parameters such as radius of curvature, thickness, semi diameter, glass type and optionally tilt and decenter. Before we proceed, we notice that the human eye can only distinguish aberrations up to the fourth or fifth order. When we design the lens we have to take in consideration the aberrations, the aberration correction and the design considerations.
We design a singlet, a doublet and an apchromat. We are interested about resolution of these lenses configurations. A singlet has chromatic aberration; a doublet can focus two wavelengths and an apochromat can focus three wavelengths (Geary, 2002). Therefore, the

type of the lenses that are used in our analysis has significant impact on the shape and resolution of the pulse at the output of these lenses.

3.4.1 The design of the singlet

The singlet has the lens focal length 20*mm* and $f/2$ aperture. We use the glass BK 7, and we assume the object is at infinity (M = 1). The merit functions are the axial color and the coma (Kidger, 2001, 2004), (Toadere & Mastorakis, 2010). To solve this problem we must solve the equation system (figure 4):

$$\begin{cases} f_1 = \phi - \phi_1 \\ f_2 = \dfrac{1}{2}\phi^2 L(a_5 B - a_6 M) \end{cases} \tag{33}$$

where:
ϕ is the power of the lens.

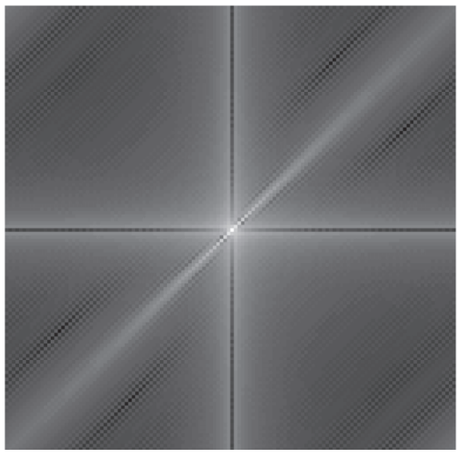

Fig. 4. The log of the PSF for the singlet

3.4.2 The design of an achromatic doublet

The achromatic doublet has the focal length 23*mm* with an *f/2* aperture. Assume the object is at infinity (M =1). We use the glasses BK 7 and SF 2. The merit functions are coma and spherical aberrations (Kidger 2001, 2003), (Geary, 2002). To solve this problem we must solve the equations system (figure 5):

$$\begin{cases} f_1 = \phi - (\phi_1 + \phi_2) \\ f_2 = \dfrac{\phi_1}{v_1} + \dfrac{\phi_2}{v_2} \end{cases} \tag{34}$$

where:
ϕ_1 is the power of the first lens,
ϕ_2 is the power of the second lens,
v_1 , v_2 are the corresponding Abbe numbers.

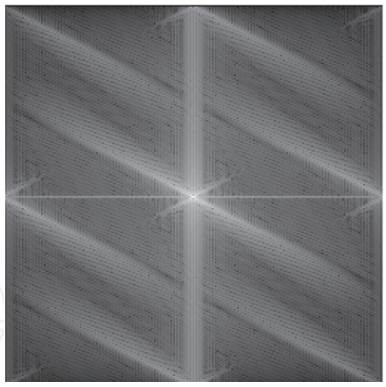

Fig. 5. The log of the PSF for the achromatic doublet

3.4.3 The design of an apochromat

The apochromat has the lens focal length 20*mm* with an *f*/2 aperture. We use the glass F2, KZFSN5, FK51, and we assume the object is at infinity (M = 1). The merit functions are spherical aberration and the axial color (Kidger 2001, 2004), (Geary, 2002). To solve this problem we must solve the equation system (figure 6):

$$\begin{cases} f_1 = \phi - \phi_1 + \phi_2 + \phi_3 \\ f_2 = \left(\frac{1}{\nu_1}\right)\phi_1 + \left(\frac{1}{\nu_2}\right)\phi_2 + \left(\frac{1}{\nu_3}\right)\phi_3 \\ f_3 = \left(\frac{P_1}{\nu_1}\right)\phi_1 + \left(\frac{P_2}{\nu_2}\right)\phi_2 + \left(\frac{P_3}{\nu_3}\right)\phi_3 \end{cases} \tag{35}$$

where:

ϕ_1, ϕ_2, ϕ_3 are the powers of the elements,

v_1, v_2, v_3 are the Abbe numbers,

P_1, P_2, P_3 are the partial dispersions.

The first equation determines the power, the second equation the axial color and the third equation the longitudinal color.

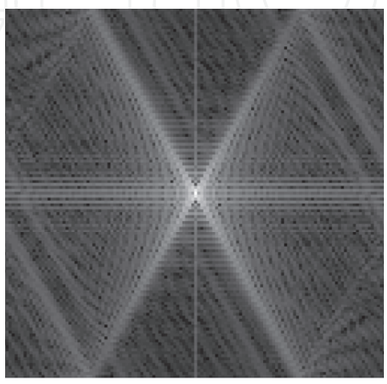

Fig. 6. The log of PSF for the apochromat

4. The optical fiber

An optical fiber is a thin, flexible and transparent fiber that acts as a waveguide in order to transmit light between the two ends of the fiber. During the radiation propagation trough the optical fiber it suffers of material dispersion, modal dispersion and polarization dispersion. Happily there are different types of fibers which allow us to reduce the modal dispersion and the polarization dispersion. Material dispersion is a problem that can be solved only by the designer and the producer of the fiber. When we make the physical model of the refraction index of the fibers we take in consideration the modal dispersion and the polarization dispersion. Modal dispersion happens in multimode fibers. Usually, the waveguide effect is achieved using in the core of the fiber a refractive index that is slightly higher than the refraction index of the surrounding cladding.
In order to reduce the effect of the modal dispersion, we analyze the functionality of the graded index fiber, the step index fiber and the fiber based on self caring effect. The step and graded index fibers use a linear refractive index and the fiber with self caring effect use a non linear refractive index. Polarization gives us information about linear and nonlinear comportment of the refractive index of the fibers. The polarization is deduced from the Maxwell equations.

4.1 The Maxwell equations

The Maxwell equations are (Mitsche, 2009), (Poon & Banarje, 2001), (Poon & Kim, 2006):

$$\nabla \cdot \vec{D} = 0 \tag{36}$$

$$\nabla \cdot \vec{B} = 0 \tag{37}$$

$$\nabla \times \vec{B} = \mu_0 \frac{\partial \vec{D}}{\partial t}, \tag{38}$$

$$\nabla \times \vec{E} = -\frac{\partial \vec{B}}{\partial t} \tag{39}$$

and:

$$\vec{D} = \varepsilon_0 \vec{E} + \vec{P}, \tag{40}$$

$$\vec{B} = \mu_0 \left(\vec{H} + \vec{M} \right), \tag{41}$$

$$\vec{j} = \sigma \vec{E} \tag{42}$$

where:

$\vec{E}$ is the electric field strength (V / m),

$\vec{H}$ is the magnetic field strength (A / m),

$\vec{D}$ is dielectric displacement (As / m^2),

$\vec{B}$ is the magnetic induction (Vs / m^2),

$\vec{J}$ is the current density (A / m^2),

$\vec{P}$ is the polarization,

$\vec{M}$ is the magnetization,

σ is the conductivity.

We rearrange the equation (39) using the equation (40):

$$\nabla \times \nabla \times \vec{E} = \nabla \times \left(-\frac{\partial \vec{B}}{\partial t} \right), \tag{43}$$

$$\nabla\left(\nabla \cdot \vec{E}\right) - \nabla^2 \vec{E} = -\frac{\partial}{\partial t}\left(\nabla \times \vec{B}\right),$$

$$\nabla\left(\nabla \cdot \vec{E}\right) - \nabla^2 \vec{E} = -\frac{\partial}{\partial t}\left(\mu_0 \frac{\partial \vec{D}}{\partial t} \right),$$

$$\nabla\left(\nabla \cdot \vec{E}\right) - \nabla^2 \vec{E} = -\mu_0 \frac{\partial^2 \vec{D}}{\partial t^2},$$

$$\nabla\left(\nabla \cdot \vec{E}\right) - \nabla^2 \vec{E} = -\mu_0 \frac{\partial^2}{\partial t^2}\left(\varepsilon_0 \vec{E} + \vec{P}\right),$$

$$\nabla\left(\nabla \cdot \vec{E}\right) - \nabla^2 \vec{E} = -\mu_0 \varepsilon_0 \frac{\partial^2 \vec{E}}{\partial t^2} - \mu_0 \frac{\partial^2 \vec{P}}{\partial t^2}. \tag{44}$$

If $\vec{E} \| \vec{P}$ and $D \| E$, it fallows that $\nabla \vec{D} = \nabla \vec{E} = 0$ and the equation (44) becomes:

$$\nabla^2 \vec{E} = \mu_0 \varepsilon_0 \frac{\partial^2 \vec{E}}{\partial t^2} + \mu_0 \frac{\partial^2 \vec{P}}{\partial t^2}. \tag{45}$$

The polarization is express as (Mitsche, 2009), (Poon & Banarje, 2001), (Poon & Kim, 2006):

$$P = \varepsilon_0 \left(\chi^{(1)} \vec{E} + \chi^{(2)} \vec{E}^2 + \chi^{(3)} \vec{E}^3 + ... \right). \tag{46}$$

4.2 The linear refractive index

For the linear case we take from equation (46) only the linear term:

$$P = \varepsilon_0 \chi^{(1)} \vec{E}. \tag{47}$$

Using equation (47) we rewrite the equation (40):

$$\vec{D} = \varepsilon_0 \vec{E}\left(1 + \chi^{(1)}\right). \tag{48}$$

In equation (48) the term inside the brackets represents the dielectric constant:

$$1+\chi^{(1)}=\varepsilon=\left(n+i\frac{C}{2\omega}\alpha\right)^2 \tag{49}$$

where:
n is the index of refraction,
α is the coefficient of absorption.
In equation (49) if $\alpha\approx 0$ then:

$$\varepsilon=n^2\,. \tag{50}$$

Having these conditions we insert the equation (47) in to equation (45) and we obtain the linear wave equation (Mitsche, 2009), (Poon & Banarje, 2001):

$$\nabla^2\vec{E}=\frac{n^2}{c^2}\frac{\partial^2}{\partial t^2}\vec{E}\,, \tag{51}$$

and equivalently for the magnetic field:

$$\nabla^2\vec{H}=\frac{n^2}{c^2}\frac{\partial^2}{\partial t^2}\vec{H}\,. \tag{52}$$

4.2.1 Optical propagation through the step index fiber

Step-index fibers are optical fibers with the simplest possible refractive index profile: a constant refractive index n_1 in the core with some radius r, and another constant value n_2 in the cladding (Mitsche, 2009):

$$n_1>n_2\,, \tag{53}$$

$$n_2\cong n_1(1-\Delta)\,, \tag{54}$$

where:
$\Delta=\frac{n_1-n_2}{n_1}$ is the fractional change in the index of refraction,
n_1 is the refractive index in the core,
n_2 is the refractive index in the cladding.
By construction, this type of optical fiber has constant index of refraction in the core. This fact leads to the apparition of the modal dispersion during the propagation of the Gaussian pulse trough the step index fiber. At the output of the fiber the shape of the pulse is spread which produce intensity attenuation. Consequently, this type of optical fiber has modest performances.

4.2.2 Optical propagation through the graded index fiber

A graded-index fiber is an optical fiber whose core has a refractive index that decreases with increasing radial distance from the fiber axis. The index profile is very nearly parabolic. The advantage of the graded-index is the considerable decrease in modal dispersion ensuring a constant propagation velocity for all light rays (Mitsche, 2009):

$$n(x,y) = n_0\left[1 + \Delta(x,y)\right] \tag{55}$$

where:
n_0 is the intrinsic refractive index of the medium,
$n(x,y)$ is the medium index of refraction in the location (x,y),
$\Delta(x,y)$ is the variation of $n(x,y)$.
In reference (Poon & Kim, 2006) is presented a beautiful demonstration in which a plane wave propagates trough a graded index fiber. After the plane wave is substitute in the wave equation, the equation is solved and the results are the Hermite Gaussian polynomials. Since we have total mathematical compatibility with the equation (1), the only concern should be related to the propagation trough the refractive index. Due to the periodic focusing by the graded index, the distribution of the Gaussian pulse does not deform during its propagation through the fiber. This means that the Gaussian spatial confining of the light wave is preserved as the light propagates through the fiber. Therefore, the fiber preserves the spatial resolution of the original Gaussian pulse.

4.3 The nonlinear refractive index

For the nonlinear case (Mitsche, 2009), (Poon & Banarje, 2001), (Poon & Kim, 2006) using the equation (46), the polarization is express taking in consideration the first nonlinear and non zero term:

$$P = \varepsilon_0\left(\chi^{(1)}\vec{E} + \chi^{(3)}\vec{E}^3\right) \tag{56}$$

the second term in the expression (46) vanishes due to the statistical glass structure.
Using equation (50) we express the nonlinear term as:

$$\varepsilon = n^2 = 1 + \chi^{(1)} + \chi^{(3)}E^2 = \varepsilon_{linear} + \chi^{(3)}E^2\,, \tag{57}$$

$$\varepsilon = \varepsilon_{linear}\left(1 + \frac{\chi^{(3)}E^2}{\varepsilon_{linear}}\right). \tag{58}$$

In this condition the refractive index is:

$$n = n_0\sqrt{1 + \frac{\chi^{(3)}E^2}{\varepsilon_{linear}}} \approx n_0\left(1 + \frac{\chi^{(3)}E^2}{2n_0^2}\right) \tag{59}$$

where:
n_0 is the refractive index at zero intensity.
We note the term:

$$n_2 = \frac{\chi^{(3)}}{2n_0}\,, \tag{60}$$

$$n = n_0 + n_2 E^2 , \tag{61}$$

or:

$$n = n_0 + n_2 I , \tag{62}$$

where:
n_0 is the refractive index at zero intensity,
n_2 is the Kerr coefficient.

4.3.1 Wave propagation in a nonlinear inhomogeneous medium

The wave propagation in a nonlinear inhomogeneous medium (Poon & Kim, 2006) is governed by the combination of self phase modulation due to the Kerr effect and the group velocity dispersion which balance out each others and can lead to solitons (self sustaining pulses). The optical pulse propagates into a fiber whose index of refraction depends on the pulse intensity. The index of refraction is given by the equation (62). This type of fiber ensures the best propagation conditions. At the output of the fiber the pulse preserves its shape and also it is amplified in intensity.

5. The CMOS sensor

The image at the output of the optical fiber is projected on the image sensor. In this analysis we use a passive pixel complementary metal oxide semiconductor (PPS CMOS). We analyze the modulation transfer function (MTF) of the CMOS and the electrical part of the CMOS considering the photon shot noise and the fixed pattern noise (FPN). Finally, we use a Lapacian filter, an amplitude filter and a bilateral filter in order to reconstruct the noisy blurred image.

5.1 The optical part of a PPS CMOS sensor

The PPS CMOS image capture sensors it is a complex device which converts the focalized light in to numerical signal. CMOS image sensors consists of a $m \times n$ array of pixels; each pixel contains: the photodetector that converts the incident light in to photocurrent, the circuits for reading out photocurrent; part of the readout circuits are in each pixel, the rest are placed at the periphery of the array. CMOS sensors integrate on the same chip the capture and processing of the signal (Holst & Lomheim, 2007).
In our analyses we use a pixel made in $0.5\mu m$ technologies. To model the sensor response as a linear space invariant system, we assume the *n+/p-sub* photodiode with very shallow junction depth, and therefore we can neglect generation in the isolated *n*+ regions and only consider generation in the depletion and *p*-type quasi-neutral regions. We assume a uniform depletion region. The parameters values of the pixel are: $z = 5.4\mu m$, $L_d = 4\mu m$, $L = 10\mu m$, $w = 4\mu m$, $\lambda = 550nm$. 1/2 inch CMOS with C optical interface is selected, i.e. its back working distance is 23 ± 0.18 mm. The visual band optical system has 60° field of view (FOV), f/number 2.5 (Toadere, 2010).
In figure 7 we have the cross section of a pixel and we can see that it is part of a periodic structure of pixels. The picture presents a structure of a complex device compound from the lenses , the colors filters and the analog part responsible with the conversion from

photons to charges and then in to voltage. Supplementary, not represented in the figure, we have conversion from analog signal to digital signal and numeric colors processing on the same chip.

The photodiodes are semiconductor devices responsive with capture of photons. They absorb photons and convert them in to electrons. The collected photons increase the voltage across the photodiode, proportional with the incident photon flux. The photodiodes work by direct integration of the photocurrent and dark current. They should have appropriate FOV, fill factor, quantum efficiencies and pixel dimension for the sensitive array. A good light capture allows sensor to obtain a high dynamic range scene.

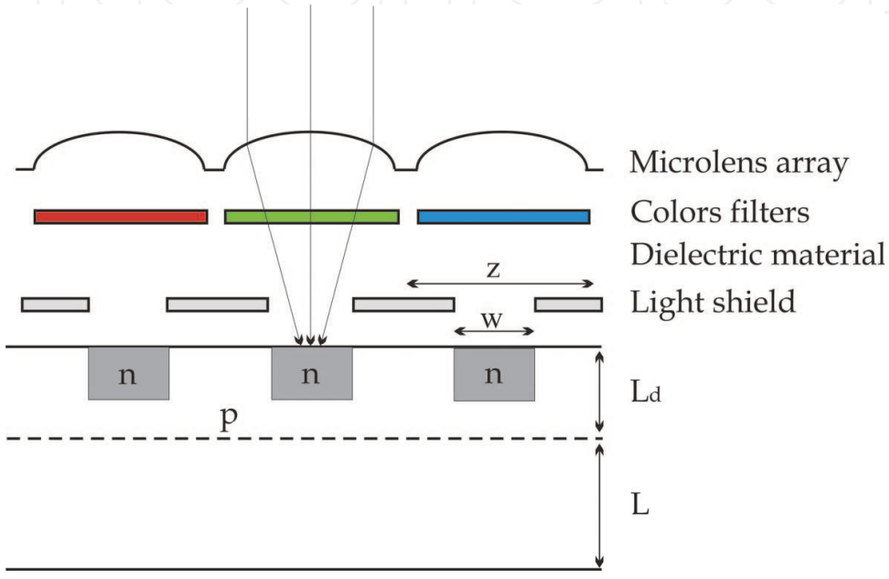

Fig. 7. The view of the simplified pixel cross section

z is the distance between pixel,
w is the pixels width,
L is the quasi neutral region,
L_d is the depletion length.

5.1.1 The modulation transfer function of the CMOS image sensors

The sharpness of a photographic imaging system or of a component of the system (the lens and the optical part of CMOS) is characterized by the MTF, also known as spatial frequency response. The optical part of the CMOS is characterized by its afferent MTF (Holst & Lomheim 2007). The contrast in an image can be characterized by the modulation:

$$M = \frac{s_{\max} - s_{\min}}{s_{\max} + s_{\min}} \tag{63}$$

where:

$s_{\max}$ and $s_{\min}$ are the maximum and minimum pixel values over the image.

Note that $0 \le M \le 1$. Let the input signal to an image sensor be a 1D sinusoidal monochromatic photon flux:

$$F(x,f) = F_0\left[1+\cos(2\pi fx)\right] \tag{64}$$

for $0 \le f \le f_{Nyquist}$.

The sensor modulation transfer function is defined as:

$$MTF(f) = \frac{M_{out}(f)}{M_{in}(f)} \tag{65}$$

from the definition of the input signal $M_{in} = 1$. MTF is difficult to find analytically and is typically determined experimentally. For the beginning we made a 1D analysis for simplicity and at the end we generalize the results to 2D model, which we will use in our analyses.

By making several simplifying assumptions, the sensor can be modeled as a 1D linear space-invariant system with impulse response *h*(*x*) that is real, nonnegative, and even. In this case the transfer function (Toadere & Mastorakis, 2010):

$$H(f) = F\left[h(x)\right] \tag{66}$$

is real and even, and the signal at *x* is:

$$S(x) = F(x,f) * h(x), \tag{67}$$

$$S(x) = F_0\left[1+\cos(2\pi fx)\right] * h(x),$$

$$S(x) = F_0\left[H(0)+H(f)\cos(2\pi fx)\right],$$

therefore:

$$S_{\max} = F_0\left[H(0)+\left|H(f)\right|\right], \tag{68}$$

$$S_{\min} = F_0\left[H(0)-\left|H(f)\right|\right], \tag{69}$$

and the sensor MTF is given by:

$$MTF(f) = \frac{\left|H(f)\right|}{H(0)}. \tag{70}$$

In figure 7 we have a 1-D doubly infinite image sensor. To model the sensor's response as a linear space-invariant system, we assume *n+/p-sub* photodiode with very shallow junction depth, and therefore we can neglect generation in the isolated *n*+ regions and only consider generation in the depletion and *p*-type quasi-neutral regions. We assume a uniform depletion region (from $-\infty$ to ∞). In figure 8, the monochromatic input photon flux $F(x)$ to the pixel current $iph(x)$ can be represented by the linear space invariant system. $iph(x)$ is sampled at regular intervals *z* to get the pixels photocurrents.

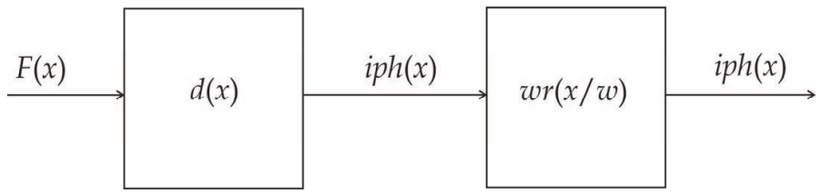

Fig. 8. The process of photogeneration and integration

$$r\left(\frac{x}{w}\right)=\begin{cases}1 & |x|\le\dfrac{w}{2}\\ 0 & otherwise\end{cases} \tag{71}$$

$d(x)$ is the spatial impulse response corresponding to the conversion from photon flux to photocurrent density. We assume a square photodetector and the impulse response of the system is thus given by:

$$h(x)=d(x)*\omega r\left(\frac{x}{\omega}\right) \tag{72}$$

and its Fourier transform (transfer function) is given by:

$$H(f)=D(f)\omega^2\sin c(\omega f) \tag{73}$$

where:

$D(0)=n(\lambda)$,

$n(\lambda)$ is the spectral response.

The spectral response is a fraction of the photon flux that contributes to photocurrents as a function of wave length. $D(f)$ can be viewed as a generalized spectral response (function of spatial frequency as well as wavelength).

After some calculus we get $D(f)$ as:

$$D(f)=\frac{q\left(1+\alpha L_f-e^{\alpha L_d}\right)}{1+\alpha L_f}-\frac{qL_f\alpha e^{\alpha L_d}\left(e^{\alpha L}-e^{\frac{L}{L_f}}\right)}{\left(1-\left(\alpha L_f\right)^2\right)\sinh\left(\dfrac{L}{L_f}\right)}, \tag{74}$$

$$H(f)=D(f)w^2\sin c(wf), \tag{75}$$

the modulation transfer functions for $|f|\le\dfrac{1}{2p}$ is:

$$MTF(f)=\frac{|H(f)|}{H(0)}=\frac{D_f}{D_0}w^2\sin c(wf) \tag{76}$$

$\frac{D_f}{D_0}$ is called the diffusion MTF and $\sin c(wf)$ is called the geometric MTF.

Consequently, we have:

$$MTF_{CMOS} = MTF_{diffu\sin} \cdot MTF_{geometric} . \tag{77}$$

But in our analyses we use 2D signals so we must generalize 1D case to 2D case. We know that we have square aperture with length w for each photodiode:

$$MTF(f_x, f_y) = \frac{|H(f_x, f_y)|}{H(0)}, \tag{78}$$

$$MTF(f_x, f_y) = \frac{D_{(f_x, f_y)}}{D_0} w^2 \sin c(wf_x) \sin c(wf_y), \tag{79}$$

where:

f_x is the spatial frequency on x direction,

f_y is the spatial frequency on y direction.

Spatial frequency (lines/mm) is defined as the rate of repetition of a particular pattern in unit distance. It is indispensable in quantitatively describing the resolution power of a lens. The first level in a CMOS image sensor is a lens which focuses the light on each pixel photodiode.

In figure 9 we have the graphical representation of the $MTF(f)$ calculated in equation (79).

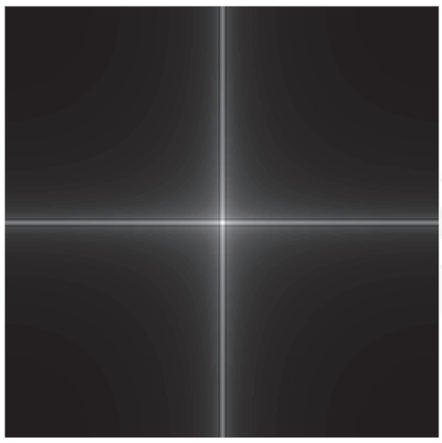

Fig. 9. The log of the PSF for the CMOS sensor

Diffusion MTF decreases with the wavelength. The reason is that the quasi-neutral region is the first region of absorption, and therefore photogenerated carriers due to lower wavelength photons (which are absorbed closer to the surface) experience more diffusion than those generated by higher wavelengths.

5.2 The electrical part of the PPS CMOS sensor

The PPS CMOS image sensor consists of a $n \times m$ PPS array. They are based on photodiodes without internal amplification. In these devices each pixel consists of a photodiode and a transistor in order to connect it to a readout structure (figure 10.). Then, after addressing the pixel by opening the row-select transistor, the pixel is reset along the bit line. The readout is performed one row at a time. At the end of integration, charge is read out via the column charge to voltage amplifiers. The amplifiers and the photodiodes in the row are then reset before the next row readout commences. The main advantage of PPS is its small pixel size. In spite of the small pixel size capability and a large fill factor, they suffer from low sensitivity and high noise due to the large column's capacitance with respect to the pixel's one. Also during the signal propagation trough the bit configuration it suffers of temporal noises perturbations (Holst & Lomheim 2007), (Toadere & Mastorakis, 2010), (Toadere, 2010).

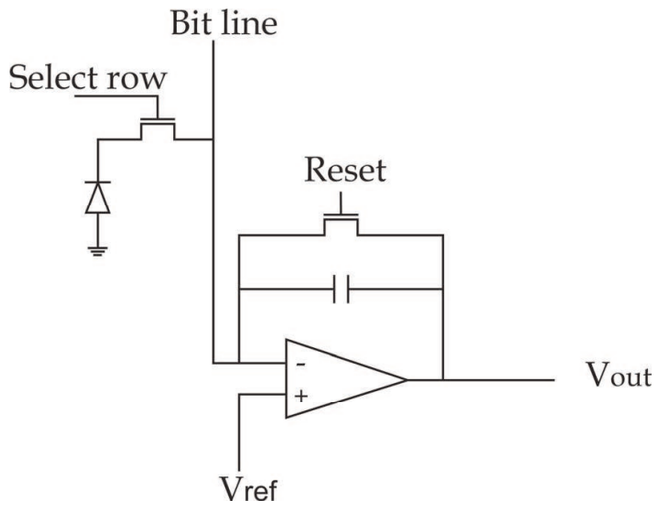

Fig. 10. A schematic of a passive pixel sensor

The pixel photodiode works by direct integration of the photocurrent and dark current on the photodiode condenser during the integration time. At the end of the integration time the condenser charge is read out by the next electronic block.

$$Q_{t\,\mathrm{int}} = \left(i_{ph} + i_{dc}\right) t_{\mathrm{int}}\,, \tag{80}$$

$$i_{ph} = q \int f(\lambda)\eta(\lambda)\, d\lambda\,, \tag{81}$$

where:

$q = 1.6 \times 10^{-19} C$ is the electron charge,

i_{ph} is the photodiode current,

i_{dc} is the dark current.

Dark current i_{dc} is the leakage current and it corresponds to the photocurrent under no illumination. It can not be accurately determined analytically or using simulation tools. Fluctuate with temperature and introduces unavoidable photon shot noise. The photon shot

noise, dark current noise and thermal noise are signal dependent noises; reset and offset noises are signal independent noises.

5.2.1 The electrical noises

Image noise is a random, usually unwanted, variation in brightness or color information in an image. In a CMOS sensor image noise can originate in electronic noise that can be divided in temporal and FPN or in the unavoidable shot noise of an ideal photon detector. Image noise is most apparent in image regions with low signal level, such as shadow regions or underexposed images (Holst & Lomheim 2007).
The photon shot noise is generated by fluctuations in static *dc* current flow through depletion regions of a *pn* junction, resulted after the photons to electrons conversion process. The diode also suffers of dark current noise. Thermal noise is generated by thermally induced motion of electrons in the resistive regions of a MOS transistor channel in strong inversion polarization. Some time the photon shot noise and thermal noise can be considered as white Gaussian noise. In addition we have the reset, read and FPN noises due to other components electronics. Noises represent an additive process (Toadere, 2010).
Shot Noise is associated with the random arrival of photons at any detector. The lower the light levels the smaller the number of photons which reach our detector per unit of time. Consequently, there will not be continuous illumination but a bombardment by single photons and the image will appear granulose. The signal intensity, i.e. the number of arriving photons per unit of time, is stochastic and can be described by an average value and the appropriate fluctuations. The photon shot noise has the Poisson distribution:

$$P(k,\lambda)=\frac{e^{-\lambda}\lambda^{k}}{k!} \tag{82}$$

where:
$k=1\div n$, n is a non-negative integer,
λ is a positive real number.
The readout noise of a PPS CMOS is generated by the electronics and the analog-to-digital conversion. Readout noise is usually assumed to consist of independent and identically distributed random values; this is called white noise. The noise is assumed to have the normal white Gaussian distribution with mean zero and a fixed standard deviation proportional to the amplitude of the noise. The analog to digital convertor produces quantization errors. Whose effect can be approximated by uniformly distributed white noise whose standard deviation is inversely proportional to the number of bits used.

5.2.2 The fixed pattern noise

In a perfect image sensor, each pixel should have the same output signal when the same input signal is applied, but in image sensors the output of each sensor is different. The FPN is defined as the pixel-to-pixel output variation under uniform illumination due to device and interconnect mismatches across the image sensor array. These variations cause two types of FPN: the offset FPN, which is independent of pixel signal, and the gain FPN or photo response non uniformity, which increases with signal level. Offset FPN is fixed from frame to frame but varies from one sensor array to another. The most serious additional source of FPN is the column FPN introduced by the column amplifiers. In general PPS has

FPN, because PPS has very large operational amplifier offset at each column. Such FPN can cause visually objectionable streaks in the image. Offset FPN caused by the readout devices can be reduced by correlated double sampling (CDS). Each pixel output is readout twice, once right after reset and a second time at the end of the integration. The sample after reset is then subtracted from the one after integration (figure 11).
For a more detailed explanation, check out the paper by Abbas El Gammal (El Gamal et al. 1998). In this paper we focus our attention in FPN effects on image quality and we do not compute the FPN, we accept the noises as they are presented in references.

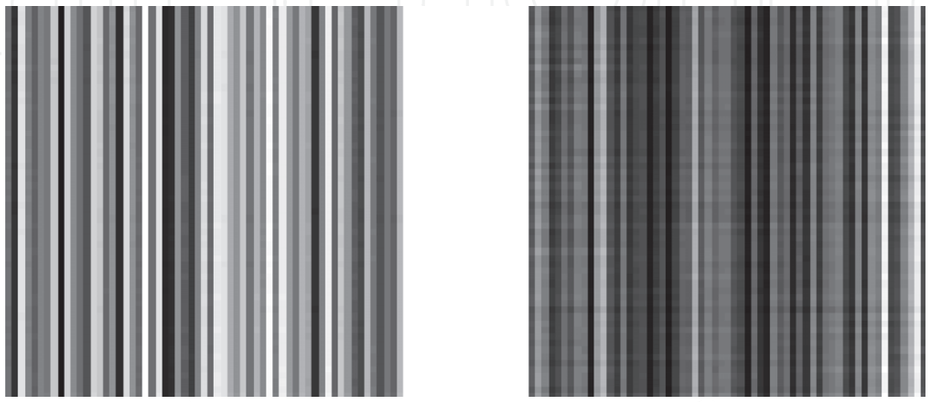

a) b)

Fig. 11. a) the FPN of the PPS without CDS, b) the FPN of the PPS with CDS

5.2.3 The dynamic range

Dynamic range is the ratio of the maximum to minimum values of a physical quantity. For a scene, the ratio is between the brightest and darkest part of the scene. The dynamic range of a real-world scene can be 100000:1. Digital cameras are incapable of capturing the entire dynamic ranges of scenes, and monitors are unable to accurately display what the human eye can see. The sensor dynamic range (*DR*) quantifies its ability to image scenes with wide spatial variations in illumination. It is defined as the ratio of a pixel's largest nonsaturating photocurrent $i_{\max}$ to its smallest detectable photocurrent $i_{\min}$ or the ratio between full-well capacity and the noise floor**.** The maximum amount of charge that can be accumulated on a photodiode capacitance is called full-well capacity. The initial and maximum voltages are V_{reset} and $V_{\max}$, they depend on the photodiode structures and operating conditions (Holst & Lomheim, 2007), (Toadere, 2010)**.** The largest saturating photocurrent is determined by the well capacity and integration time t_{int} as:

$$i_{\max} = \frac{qQ_{\max}}{t_{\text{int}}} - i_{dc} \tag{83}$$

the smallest detectable signal is set by the root mean square of the noise under dark conditions. *DR* can be expressed as:

$$DR = 20\log_{10}\frac{i_{\max}}{i_{\min}} = 20\log_{10}\frac{qQ_{\max} - i_{dc}t_{\text{int}}}{\sqrt{qt_{\text{int}}i_{dc} + q(\sigma_{read}^2 + \sigma_{DNSU}^2)}} \tag{84}$$

where:

$Q_{\max}$ is the effective well capacity,

σ_{read}^2 is the readout circuit noise.

σ_{DNSU}^2 is the offset *FPN* due to dark current variation, commonly referred to as *DSNU* (dark signal non-uniformity).

5.2.4 The analog to digital conversion

The analog to digital conversion is the last block of the analog signal processing circuits in the CMOS image sensor. In order to convert the analog signal in to digital signal we compute the: analog to digital curve, the voltage swing and the number of bits. The quality of the converted image is good and the image seams to be unaffected by the conversion (Holst & Lomheim, 2007), (Toadere, 2010).

6. The image reconstruction

In the process of radiation capture with our proposed image acquisition system, the input photon flux is deteriorated by the combined effects of the optical aberrations and electrical noises. The optics is responsible for colors fidelity and spatial resolution; the electronics introduce temporal and spatial electrical noises. At the output of the electrical part the image is corrupted by the optical blur and the combined effect of the FPN and the photon shot noise. In order to reduce the blur we use a Laplacian filter, to reduce the FPN we use a frequencies amplitude filter which block the spikes spectrum of the FPN. Finally we reject the remains noise using a bilateral filter.

6.1 The Laplacian filter

In order to correct the blur and to preserve the impression of depth, clarity and fine details we have to sharp the image using a Laplacian filter. A Laplacian filter is a 3x3 pixel mask:

$$L = \begin{bmatrix} 0 & -1 & 0 \\ -1 & 4 & -1 \\ 0 & -1 & 0 \end{bmatrix}. \tag{85}$$

To restore the blurred image we subtract the Laplacian image from the original image (Toadere, 2010), (Toadere & Mastorakis, 2010).

6.2 The amplitude filter

The FPN is introduced by the sensor's column amplifiers and consists of vertical stripes with different amplitudes and periods. Such type of noise in the Fourier plane produces a set of spikes periodic orientate. A procedure to remove this kind of noise is to make a transmittance mask in Fourier 2D logarithm plane. The first step is to block the principal components of the noise pattern. This block can be done by placing a band stop filter $H(u,v)$ in the location of each spike. If $H(u,v)$ is constructed to block only components associated with the noise pattern, it fallows that the Fourier transform of the pattern is given by the relation (Yzuka, 2008), (Toadere, 2010), (Toadere & Mastorakis, 2010):

$$P(u,v) = H(u,v)\log\left[G(u,v)\right] \tag{86}$$

$G(u,v)$ is Fourier transform of the corrupted image $g(x,y)$.
After a particular filter has been set, the corresponding pattern in the spatial domain is obtained making the inverse Fourier transform:

$$p(x,y) = F\left\{\exp\left[P(u,v)\right]\right\}. \tag{87}$$

6.3 The bilateral filter

In order to reduce the remains noise, after the amplitude filter, we use a bilateral filter. It extends the concept of Gaussian smoothing by weighting the filter coefficients with their corresponding relative pixel intensities. Pixels that are very different in intensity from the central pixel are weighted less even though they may be in close proximity to the central pixel. This is effectively a convolution with a non-linear Gaussian filter, with weights based on pixel intensities. This is applied as two Gaussian filters at a localized pixel, one in the spatial domain, named the domain filter, and one in the intensity domain, named the range filter (Toadere, 2010), (Toadere & Mastorakis, 2010).

7. The result of simulations

All the blocks presented in this chapter are taken in consideration in our simulations. Although the CMOS sensor has the Bayer color sampling and interpolation, we did not take in consideration these blocks because we work with black and white images. The figure 12 presents the propagation of the laser pulse through the singlet, the step index fiber and the CMOS sensor. The figure 13 presents the propagation of a laser pulse through the achromatic doublet, the graded index fiber and the CMOS sensor. The figure 14 presents the propagation of a laser pulse through the apochromat, the self phase modulation fiber and the CMOS sensor

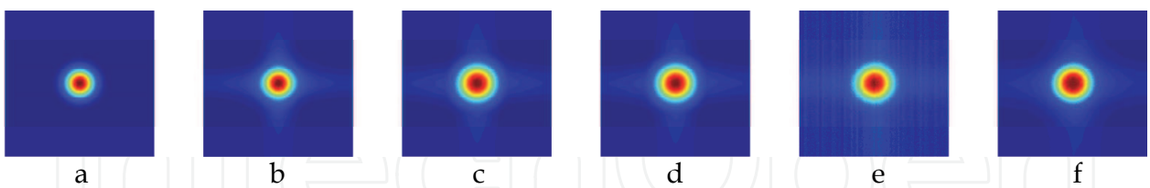

Fig. 12. The image at the output of the a) laser resonator, b) singlet, c) step fiber, d) optical part of the CMOS, e) electrical part of the CMOS, f) filtered image

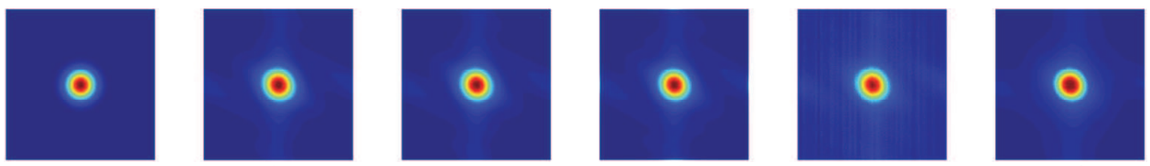

Fig. 13. The image at the output of the a) laser resonator, b) achromatic doublet, c) graded index fiber, d) optical part of the CMOS, e) electrical part of the CMOS, f) filtered image

Fig. 14. The image at the output of the a) laser resonator, b) apochromat, c) self phase modulation fiber, d) optical part of the CMOS, e) electrical part of the CMOS, f) filtered image

8. Conclusions

In this paper we simulate the propagation of a Gaussian laser pulse through different image capture systems in order to find the best configuration that preserve the shape of the pulse during its propagations. We simulate the image characteristics at the output of each block from our different systems configurations. We simulate the functionality of the singlet, the achromatic doublet and the apochromat in order to reduce the chromatic dispersion. We simulate the functionality of the step index fiber, the graded index fiber and the self phase modulation fiber in order to reduce the modal dispersion. We simulate some properties of the CMOS sensor. The sensor suffers of different noises. The purpose of this paper was to put to work together, in the same system, optical and electrical components and to recover the degraded signal. In these types of complex systems, a controlled simulation environment can provide the engineer with useful guidance that improves the understanding of design considerations for individual parts and algorithms.

9. References

Geary J. M. (2002). *Introduction to lens design with practical zemax example*, Willmann Bell, ISBN 0-943396-75-1, Richmond, USA

Goodmann J. (1996). *Introduction to Fourier optics*, McGraw-Hill, ISBN 0-07-024254-2, New York, USA

El Gamal A.; Fowler B.; Min H. & Liu X. (1998). Modeling and Estimation of FPN Components in CMOS Image Sensor, *Proceedings of SPIE, vol. 3301*, pp.168-177, San Jose, California, USA, Aprill, 1998

Holst G. C. & Lomheim T. S. (2007). *CMOS/CCD sensors and camera systems*, Spie Press, ISBN 9780970774934, Bellingham, USA

Kidger M. (2001). *Fundamental optical design*, Spie Press, ISBN 0-8194-3915-0, Bellingham, USA

Kidger M. (2004). *Intermediate optical design*, Spie Press, ISBN 0-8194-5217-3, Bellingham, USA

Mitschke F. (2009). *Fiber optics physics and technology*, Springer, ISBN 978-3-642-03702-3, Berlin, Germany

Poon T. C. & Banarje P.P. (2001). *Contemporary optical image processing with matlab*, Elseiver, ISBN: 0-08-043020-1, Oxford, UK

Poon T. C. & Kim T. (2006). *Engineering optics with matlab*, World Scientific, ISBN 981-256-872-7, Singapore

Toadere F. & Mastorakis N. (2009). Imaging a laser pulse propagation trough an image acquisition system, *Recent Advances in Circuits, Systems, Electronics, Control and Signal Processing*, pp. 93-98, ISBN: 978-960-474-139-7, Tenerife, Spain, December 14-16, 2009

Toadere F. & Mastorakis N. (2010). Simulation the functionality of a laser pulse image acquisition system, *WSEAS transaction on circuits and systems*, Issue 1, Volume 9, (January 2010), pp. 22-31, ISSN 1109-2734

Toadere F. (2010). Conversion from light in to numerical signal in a digital camera pipeline, *Proceedings of SPIE on CD ROM, Volume 7821*, Constanta, Romania, 26-28 August, 2010

Yzuka K. (2008). *Engineering Optics, Springer*, ISBN 978-0-387-75723-0, New York, USA

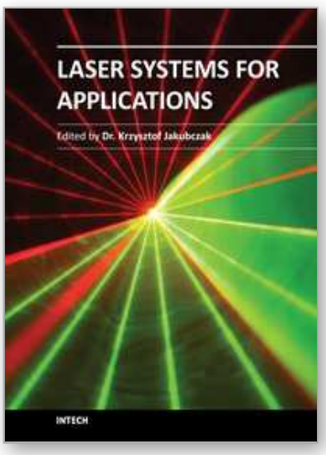

Laser Systems for Applications

Edited by Dr Krzysztof Jakubczak

ISBN 978-953-307-429-0
Hard cover, 308 pages
Publisher InTech
Published online 14, December, 2011
Published in print edition December, 2011

This book addresses topics related to various laser systems intended for the applications in science and various industries. Some of them are very recent achievements in laser physics (e.g. laser pulse cleaning), while others face their renaissance in industrial applications (e.g. CO2 lasers). This book has been divided into four different sections: (1) Laser and terahertz sources, (2) Laser beam manipulation, (3) Intense pulse propagation phenomena, and (4) Metrology. The book addresses such topics like: Q-switching, mode-locking, various laser systems, terahertz source driven by lasers, micro-lasers, fiber lasers, pulse and beam shaping techniques, pulse contrast metrology, and improvement techniques. This book is a great starting point for newcomers to laser physics.

InTech Europe
University Campus STeP Ri
Slavka Krautzeka 83/A
51000 Rijeka, Croatia
Phone: +385 (51) 770 447
Fax: +385 (51) 686 166
www.intechopen.com

InTech China
Unit 405, Office Block, Hotel Equatorial Shanghai
No.65, Yan An Road (West), Shanghai, 200040, China
中国上海市延安西路65号上海国际贵都大饭店办公楼405单元
Phone: +86-21-62489820
Fax: +86-21-62489821

IntechOpen